TRANSP simulations of International Thermonuclear Experimental Reactor plasmas

R. V. Budny, D. C. McCune, M. H. Redi, J. Schivell, and R. M. Wieland
Princeton University, Plasma Physics Laboratory, P.O. Box 451, Princeton, New Jersey 08543

(Received 13 May 1996; accepted 3 September 1996)

The TRANSP code [R. V. Budny *et al.*, Nucl. Fusion **35**, 1497 (1995)] is used to construct comprehensive, self-consistent models for plasmas within the separatrix surface in the International Thermonuclear Experimental Reactor (ITER) [*Technical Basis for the ITER Interim Design Report, Cost Review and Safety Analysis* (International Atomic Energy Agency, Vienna, 1996)]. Steady state profiles of two plasmas from the ITER ''Interim Design'' database are used. Effects of 1 MeV neutral beam injection, sawteeth mixing, toroidal field ripple, and helium ash transport are included. Results are given for the fusion rate profiles, and parameters describing effects such as the alpha particle heating of electrons and thermal ions, and the thermalization rates. The modeling indicates that the deposition of the neutral beam ions will peak in the plasma center, and the average beam ion energy will be half the injected energy. Sawtooth mixing will broaden the fast alpha profile. The toroidal ripple loss rate of alpha energy will be 3% before sawtooth crashes and will increase by a factor of 3 immediately following sawtooth crashes. Various assumptions for the thermal He transport and the He recycling coefficient at the separatrix $R_{\rm rec}$ are used. If the ratio of helium and energy confinement times, $\tau^*_{\rm He}/\tau_E$ is less than 15, the steady state fusion power is predicted to be 1.5 GW or greater. The values of the transport coefficients required for this fusion power depend on $R_{\rm rec}$. If this is larger than about 0.5, and if the inward pinch is small the required He diffusivity must be much larger than that measured in tokamaks. © *1996 American Institute of Physics.* [S1070-664X(96)02212-4]

I. INTRODUCTION

One of the goals for the International Thermonuclear Experimental Reactor (ITER) is the production of 1.5 GW of fusion power for long durations.[1,2] The required plasma conditions are far beyond those produced in current Tokamak experiments, thus considerable effort has been devoted to extrapolating scaling laws to ITER discharges. A database of possible discharges that achieve this goal of 1.5 GW is being assembled by the ITER design team.[3]

One of the crucial issues for ITER is whether the alpha heating will be sufficient to maintain ignition and the alpha particle losses will be tolerable. Good alpha confinement is necessary for self-sustained fusion reactions. Thermal alpha ash concentration must remain low so that the fuel will not be excessively depleted.

In order to predict alpha parameters, comprehensive modeling of ITER discharges is needed. The local transport must be sufficiently benign to achieve high densities and temperatures for the deuterium and tritium, and low concentrations of impurities. Large plasma currents need to be driven. Sawteeth and ripple effects need to be assessed.

To focus the modeling efforts, two of the discharges in the ITER database are used as test beds for comparing predictive modeling codes. One discharge has flat profiles and the other has moderately peaked profiles. Various predictive codes, with different strengths and weaknesses, are being used to model these discharges.

This paper describes simulations using the TRANSP plasma analysis code.[4] Although TRANSP is not primarily a predictive code, it offers a number of capabilities that complement predictive codes. These capabilities are discussed in the next section. TRANSP is used to model the high-energy neutral beam injection, sawteeth effects, toroidal field ripple effects, and helium ash concentrations. Ranges of helium ash transport that result in equilibrium ash profiles consistent with 1.5 GW of fusion power are given.

Some of the results in this paper were reported previously in a brief paper.[5]

II. TRANSP CAPABILITIES

TRANSP has a number of capabilities that make it a powerful tool for studying ITER plasma performance. These include:

General flux geometry. The geometry of the boundary (such as the 98% flux surface of diverted discharges) can be specified as a general function of time. The interior flux surfaces are computed solving the Grad–Shafranov equation. TRANSP has recently been generalized[6] to model up–down asymmetry. The boundary surface from the ITER database assumed here is designated $x=1$ in Fig. 1. The interior flux surfaces are parameterized by the square-root of the normalized toroidal flux.

Multiple species. Up to five thermal ion species can be modeled. The species that have been incorporated into TRANSP are H, D, T, He^3, He^4, Li, and an impurity of arbitrary Z and A. Several models for the relative transport of the H, D, and T are available. Explicit transport coefficients for the thermal He ash can be modeled.

Auxiliary heating and current drive. Effects of neutral beam injection (NBI), ion-cyclotron range of frequency heating (ICRF), and lower-hybrid current drive (LHCD) can be simulated. These capabilities compute the power deposition

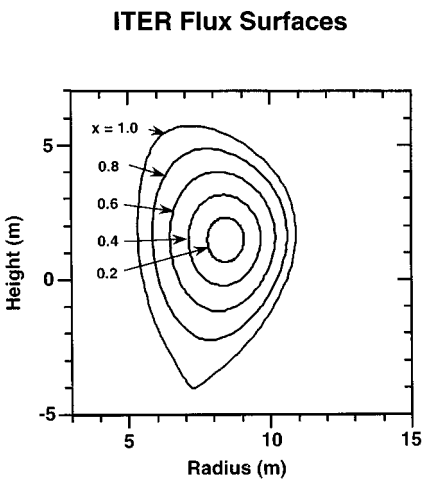

FIG. 1. Assumed boundary flux surface $x=1.0$ (for instance, for the 98% flux surface) and the interior flux surfaces calculated solving the Grad–Shafranov equation for the MHD equilibrium. The flux surfaces for both the flat and peaked categories of discharges are very similar.

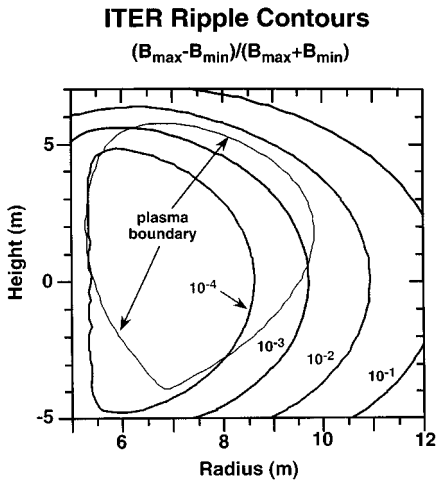

FIG. 2. Assumed toroidal ripple field and the location of the plasma boundary.

and the corresponding transport coefficients. The capabilities of simulating fast wave current drive (FWCD) and electron cyclotron heating (ECH) are being developed.

Detailed beam deposition. Monte Carlo techniques are used to model the beam deposition in three dimensions. An estimation of multistep ionization effects is included. Injection of H, D, T, and He beams can be modeled. Effects of D-NBI are discussed in Sec. IV.

Nonzero orbit effects. Monte Carlo techniques simulate orbits of alpha particles and beam ions. These give accurate simulations of the pressure and beam-driven currents in present Tokamak experiments. They are being used to study alpha parameters in the Tokamak Fusion Test Reactor (TFTR). Either neoclassical orbits, or the possible effects of anomalous fast ion diffusion can be modeled.

Fusion products modeling. The slowing down and heating of the thermal plasma by the fast alpha particles is modeled. Various losses, such as those caused by orbits intercepting the vacuum vessel are modeled.

Sawteeth effects. Models for sawteeth effects on the thermal plasma and on the fast ions have been incorporated into TRANSP.[4] These are useful for estimating q_ψ profiles and how much of the fast ions will be mixed by sawteeth crashes. Sawteeth effects are discussed in Sec. V.

Toroidal field ripple loss. A model for estimating the toroidal field ripple losses of fast ions has recently been incorporated into TRANSP.[7–9] The number and energy of the lost ions are computed. Values of the toroidal field ripple,

$$\delta(R,z)\equiv\frac{B_{\max}-B_{\min}}{B_{\max}+B_{\min}}$$

are specified. Contours of the values from the ITER database assumed here are shown in Fig. 2. Losses are discussed in Sec. VI.

Fast ion distributions. The distributions in space, energy, and pitch angle are calculated. These are useful for estimating the effects of fast ions on the magnetohydrodynamic (MHD) and toroidicity induced Alfvén eigenmodes (TAE) modes.

Coupling with MHD and TAE codes. Outputs from TRANSP runs can be used as inputs for codes such as ORBIT,[10] PEST,[11] and NOVA.[12]

Diagnostic simulations. TRANSP is capable of calculating various plasma profiles and chordal emissions along user-chosen chords. This is useful for designing diagnostics and for interpreting their results.

The TRANSP analysis code is being used extensively to analyze current tokamak experimental results from TFTR,[4,13] Joint European Torus (JET),[14] Princeton Beta Experiment-Modified (PBX-M),[15] Tokamak Experiment for Technically Oriented Research (TEXTOR),[16] TORE SUPRA,[17] and Alcator-C-Mod.[18] The widespread use of TRANSP increases its reliability and facilitates comparisons of results from different experiments. TRANSP has also been used for making predictions for future tokamak performance.[19,20]

III. BASELINE ITER SIMULATIONS

The ITER discharges are assumed to have $I_p=21$ MA and 20 toroidal field coils generating $B_{\mathrm{TF}}=5.7$ T. The boundary flux surface is assumed to have an elongation of 1.6 and a triangularity of $\cong 0.25$. The profiles used are those from the ITER ''interim'' database (ca. April, 1995) designated 1001 with flat profiles and 1002 with peaked profiles. The n_e, T_e, and T_{ion} profiles are compared in Fig. 3. The impurity profiles are calculated using the Z_{eff} profiles from the database and a choice for the Z of the impurity. The assumed profiles for Z_{eff} are shown in Fig. 4(a). The Z of the impurity is assumed to be 4.5, representing Be with $Z=4$ and a contribution from other impurities with higher Z. The radiation profiles are also given in the database, as shown in Fig. 4(b), and are used in the TRANSP modeling for calculating the electron power balance. The pressure profiles for both cases are compared in Fig. 5.

The densities of the thermal D, T, He, impurity and of the beam ions and fast alpha particles are calculated by

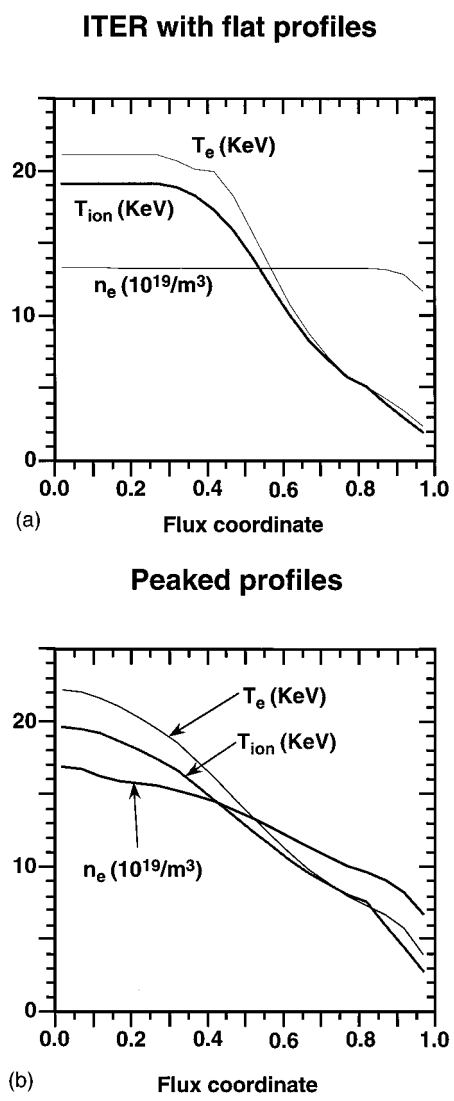

FIG. 3. Profiles of the assumed electron density, electron temperature, and ion temperature for (a) the flat and (b) the peaked cases.

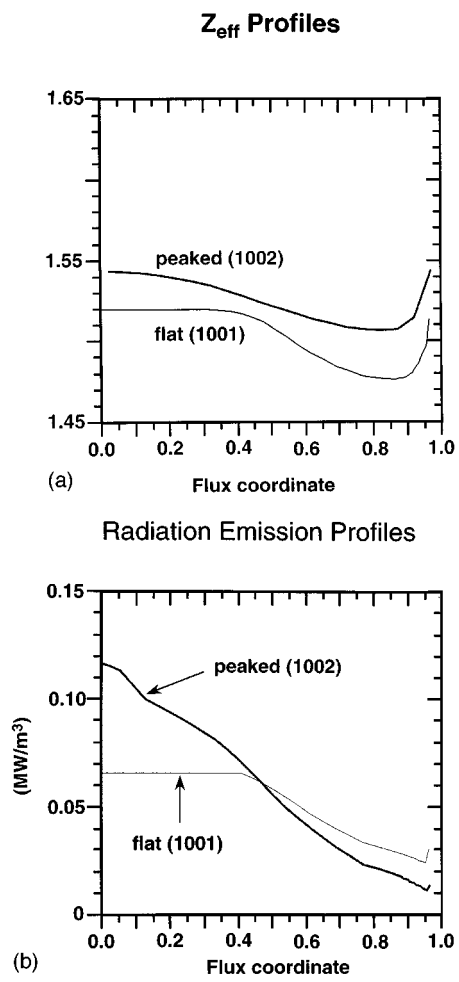

FIG. 4. Assumed profiles for (a) Z_{eff} and (b) P_{rad} for the flat and peaked density cases.

TRANSP. Several models are available for computing the relative D/T mix. The model that gives the best agreement with measurements of neutron emission profiles in TFTR has a preferential inward pinch of D relative to T.[21] This model gives pessimistic results for ITER with continual D-NBI by increasing the D density at the expense of the T density. In the following we use the more optimistic model with equal transport of the D and T. Examples of profiles are compared in Figs. 6. The computed densities of the fast ions, n_α, and n_{beam} (from 50 MW D-NBI, discussed in the next section) are relatively low, even compared to the density of the impurity, n_{imp}.

The thermal He profile n_{He} is calculated from the thermalization rate profile and the assumed He transport. Various He transport assumptions are discussed in Sec. VII. The thermal He density has a significant effect on the fusion rate by depleting the D and T densities at fixed n_e. If there were no thermal He, the fusion power from the assumed profiles would be around 2.5 GW. Results for alpha parameters for two cases with $P_{\text{DT}} \cong 1.5$ GW are summarized in Table I.

The steady-state phases of ITER discharges includes the periodic effects of sawteeth with a period assumed to be 50 s. This relatively long sawtooth period allows the q_ψ profile a long time to relax after a sawtooth crash. A short sawtooth period is predicted to reduce the perturbations of q_ψ, as dis-

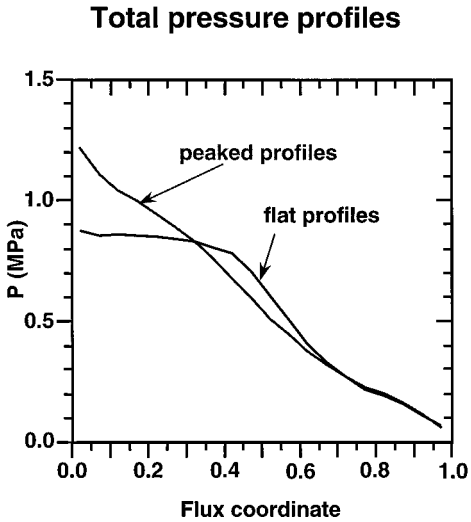

FIG. 5. Comparison of the total pressure profiles for the flat and peaked cases.

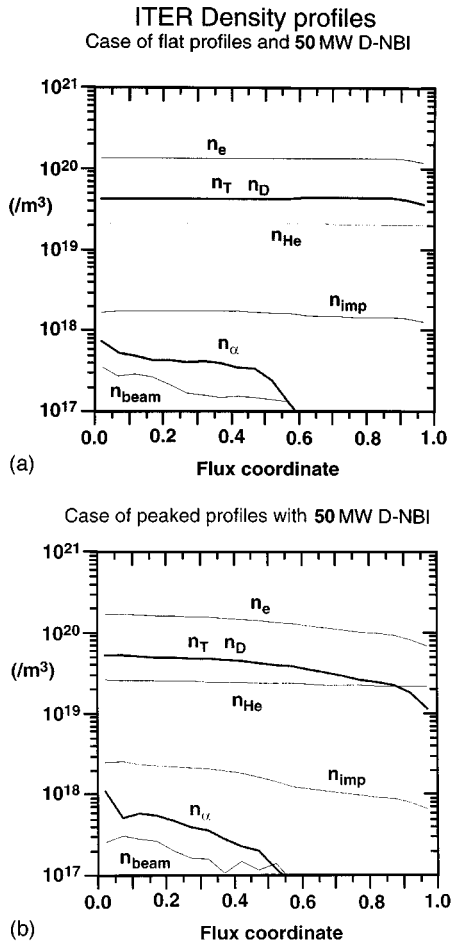

FIG. 6. Density profiles for the (a) flat and (b) peaked density cases with P_{DT}=1.5 GW and 50 MW of D-NBI at 1 MeV. The assumed electron density and the calculated thermal D, T, He and impurity, and fast D and He densities are shown.

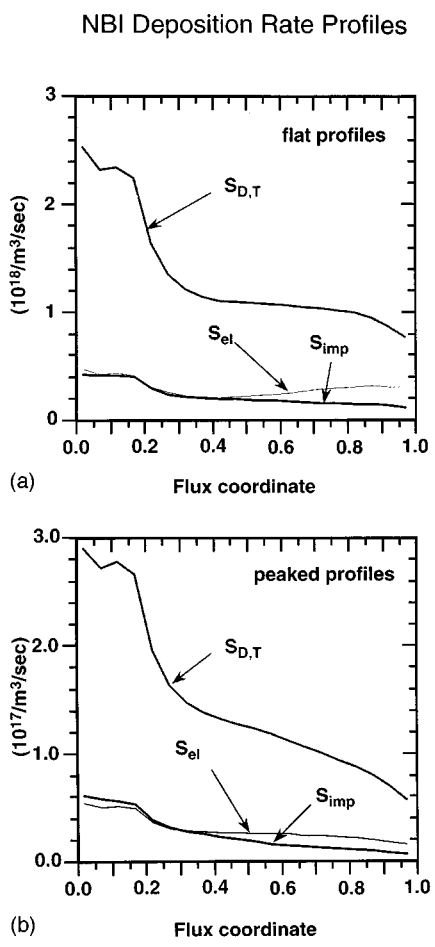

FIG. 7. Beam deposition rate profiles for the peaked density cases with 100 MW at 1 MeV for (a) flat and (b) peaked discharges. The dominant rates are ionizations of the thermal D and T, electrons, and impurities. Charge-exchange rates are lower.

cussed in Sec. V, but the increased repetition enhances the ripple loss of fast alpha particles, as discussed in Sec. VI. Approximately 120 s of these discharges are modeled in order to simulate several crashes of sawteeth, and to allow the thermal He to approach equilibrium. The NBI duration is limited to 100 s in order to provide results both with and without NBI for evaluating the effects of NBI.

IV. NEUTRAL BEAM INJECTION

The present plan for ITER is to use up to 100 MW of auxiliary heating/current drive. Some or all of this power could be D or H injection from up to three negative ion beam sources. These sources would be situated approximately 29 m from the centerline, and aimed with tangency radii of 6.5 m in the direction of the plasma current. The injected neutrals are assumed to have the full energy, which is planned to be up to 1 MeV.

This paper discusses effects of 50 MW of D-NBI. Examples for the deposition profiles are shown in Fig. 7. The dominant ionization is by collisions with the thermal D and T ions. The ionization rates by electrons and impurities are shown also. The source profiles for the fusion alphas are shown in Fig. 8.

The fast-ion distributions are calculated using Monte Carlo techniques. The profiles of the slowing down times for the fast ions (at birth) are compared in Fig. 9. The average energy of the beam ions is approximately half the injection energy, as shown in Fig. 10. The average energy of the fusion alphas is 1.5 MeV over most of the plasma profile, also shown in Fig. 10. Their average energy in the edge is higher since they are lost before they have much chance to slow down. The alpha contribution to the central pressure is 10%–15%. The beam ion contribution to the central pressure is ~2%. The beam contribution to the fusion rate is ~1%.

TRANSP calculates the beam-ion and fast alpha distributions,

TABLE I. Alpha parameters.

Parameter	Flat n_e (01001A03)	Peaked n_e (01002A07)
$\beta_\alpha(0)$	0.009	0.013
$\langle\beta_\alpha\rangle$	0.0017	0.0014
$-R^*_{\text{grad}}(\beta_\alpha)$	0.04	0.04
$n_\alpha(0)/n_e(0)$	0.003	0.006
$v_\alpha(\text{birth})/v_{\text{Alfvén}}(0)$	1.6	1.9

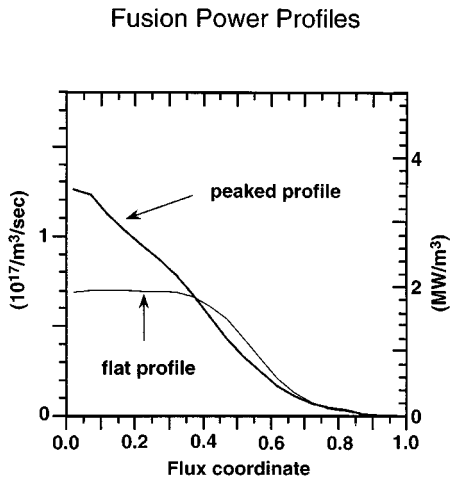

FIG. 8. Fusion power profiles for the peaked and flat density cases with P_{DT}=1.5 GW.

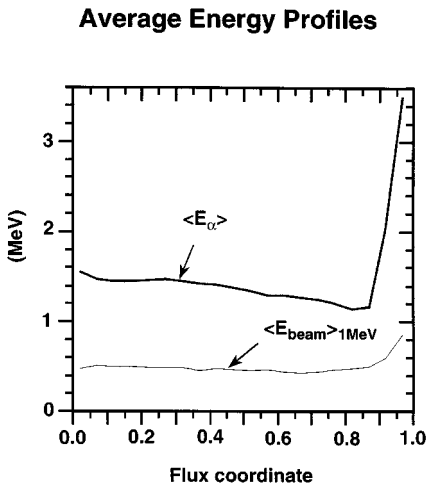

FIG. 10. Average energy profiles for the fusion alpha particles and beam ions.

$$\frac{df_j(E_j,\lambda_j,x,t)}{dV\,dE_j}$$

with dV the volume element. The independent variables are the energy E_j of the fast species j, $\lambda_j \equiv v_{\text{parallel}}/v \equiv \cos$ (pitch angle) with v_{parallel} the component of v in the direction of the plasma current, and the location in space and time. Integrating over E_j and averaging over λ gives the fast ion density. Results for 50 MW of steady state D-NBI are shown in Fig. 11. Although the beam injection is near $v_{\text{parallel}}=v$ (along the plasma current), the equilibrium distribution has considerable density at lower v_{parallel}/v.

Profiles of the plasma heating power densities during the NBI phase are shown in Figs. 12. The fusion power and heating powers of two cases are compared in Table II. Since the alpha particles are modeled to be well confined, the total alpha heating power is 20% of the total fusion power. Most of this heating is electron heating. The total beam heating and thermalization powers are 50 MW. The global and central alpha heating powers are considerably greater than the NBI heating powers since these plasmas are at ignition conditions.

The stored energies, energy confinement times, and β_{norm} values are compared in Table III. The energy confinement time is defined as the ratio of the total (thermal and fast ion) plasma energy and the total heating power. The transport coefficients of the thermal plasma which are calculated from the profile gradients and the energy, momentum, and species fluxes are shown in Figs. 13. At radii where the profiles are not decreasing monotonically, large positive or negative values for the difusivities can result. The coefficients must be lower for the cases without auxiliary heating. In the flat profile case, Fig. 13(a), χ_e and χ_{ion} are about 100 times the neoclassical value χ_{NC} over much of the profile. The exceptionally high values near the center are a consequence of the flat profiles [see Figs. 3(a) and 8]. For the peaked profile case, Fig. 13(b), the effective particle diffu-

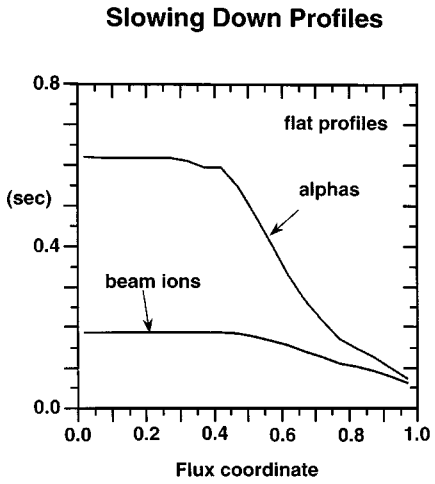

FIG. 9. Slowing down profiles for the birth alphas and beam ions.

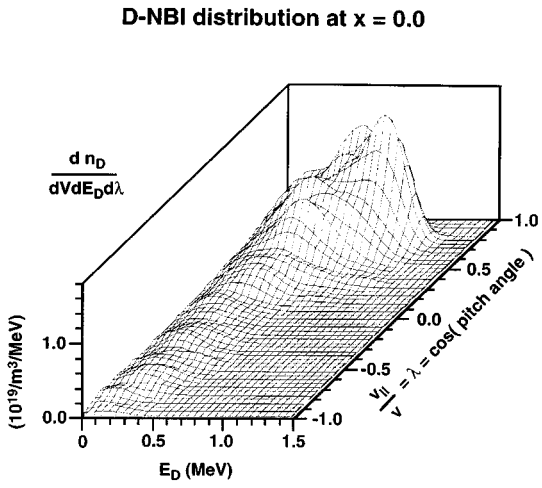

FIG. 11. Distribution in energy and λ=cos(pitch angle) at x=0.0 of the beam ions from 100 MW of 1 MeV D-NBI.

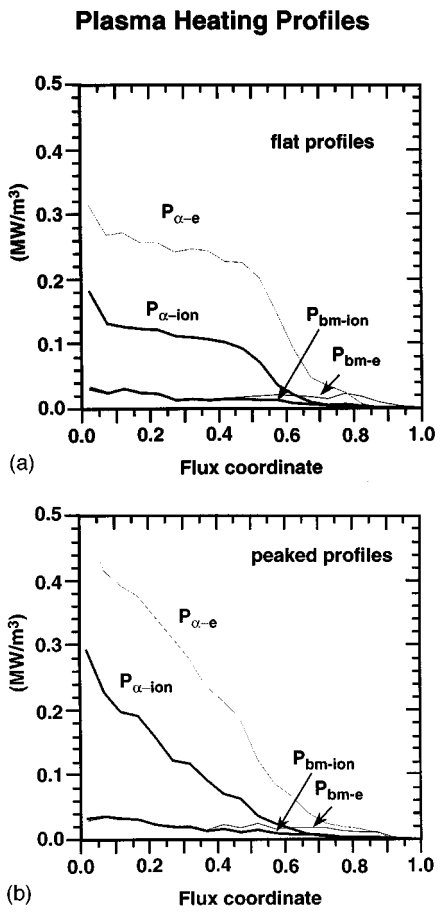

FIG. 12. Heating power density profiles for the peaked density cases with 100 MW of 1 MeV D-NBI achieving P_{DT}=1.5 GW.

sivity D_e must be considerably lower than χ_{NC}. The values for χ_e and χ_{ion} are in rough agreement with the values in the ITER interim database.

The sources of the plasma current are needed to calculate the profiles of the current profile q_ψ. The volt-second capacity may be sufficient for the Ohmic and bootstrap currents to maintain I_p=21 MA for 1000 second discharges. For steady state, a current drive system will be needed. Since the current drive mechanism has not yet been chosen, this paper assumes that the total current consists of the bootstrap, beam-driven, and Ohmic current, generated by neoclassical resistivity. The profiles shown in Fig. 14. The beam-driven current with 50 MW of D-NBI is approximately 0.6 MA. The bootstrap contributions are relatively small. Examples

TABLE II. Fusion and heating powers with 50 MW of 1 MeV D-NBI.

	Flat n_e (01001A03)		Peaked n_e (01002A07)	
	Center (MW/m^3)	Total (MW)	Center (MW/m^3)	Total (MW)
P_{DT}	2.0	1400	2.0	1400
$P_{\alpha-e}$	0.30	200	1.0	200
$P_{\alpha-l}$	0.15	78	0.50	75
P_{bm-e}	0.024	30	0.08	60
P_{bm-l}	0.025	16	0.08	35
P_{bm-th}	0.004	2	0.01	2

TABLE III. Plasma conditions with 50 MW of 1 MeV D-NBI.

Parameter	Flat n_e (01001A03)	Peaked n_e (01002A07)
W_{tot} (GJ)	1.23	1.20
W_{el} (GJ)	0.67	0.67
W_{ion} (GJ)	0.49	0.47
W_α (GJ)	0.060	0.051
W_{beam} (GJ)	0.012	0.012
τ_E (s)	4.15	4.20
β_{norm}	2.33	2.30

are compared in Table IV. A large Ohmic, or otherwise driven current is necessary to provide the total current of 21 MA.

V. SAWTEETH EFFECTS

It is not known whether ITER discharges will exhibit sawteeth, or how they will respond to sawteeth crashes. ITER sawteeth have been modeled using the PRETOR code.[22] We use TRANSP to simulate sawtooth effects on the current and fast ion profiles. For simplicity, we assume that the densities and temperatures of the thermal species are not altered, contrary to empirical observations in tokamaks.

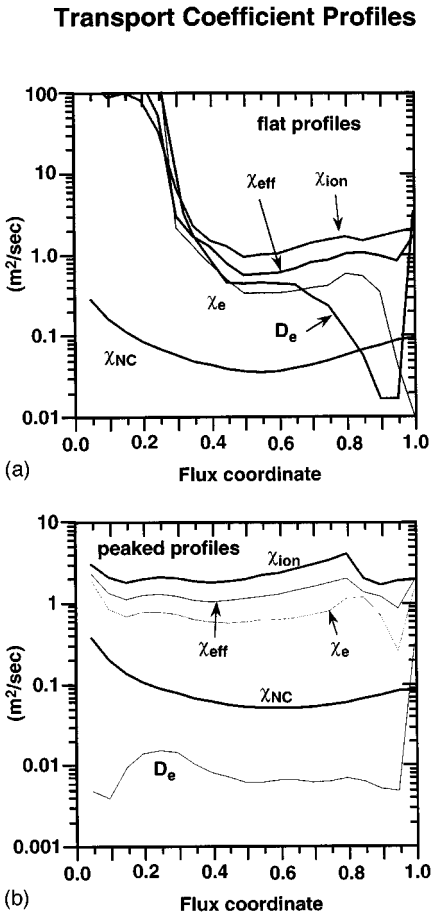

FIG. 13. Transport coefficients for the electrons and thermal ions calculated from the stored energy and heating profiles for (a) the flat density, and (b) the peaked density cases with P_{DT}=1.5 GW and 100 MW of D-NBI at 1 MeV.

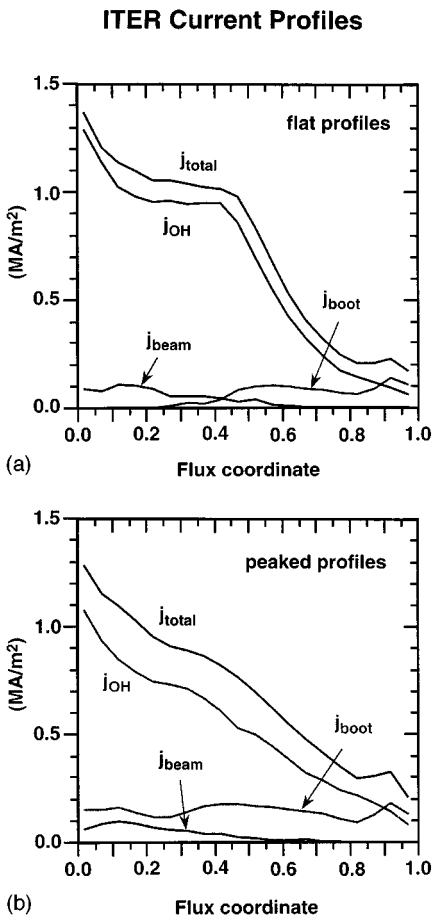

FIG. 14. Current density profiles for a peaked density case with 100 MW of 1 MeV D-NBI (a) the flat density, and (b) the peaked density cases.

The sawtooth period is assumed to be 50 s. The amount of current mixing during sawteeth crashes can be varied in TRANSP. In modeling TFTR discharges, about 20%–30% current mixing gives approximate agreement with measurements.[23] Examples of the evolutions of $q_\psi(0)$ for ITER with two different assumptions are shown in Fig. 15. If the amount of current mixing will be as small, as in TFTR, many sawteeth crashes are needed to raise $q_\psi(0)$ to values near 1. The current relaxation time is very long, so the decay of $q_\psi(0)$ after each crash is not large even with periods of 50 s. The $q_\psi=1$ surface is calculated to be around $x=0.25$–0.50. The q_ψ profiles are shown in Fig. 16.

Sawteeth affect the distribution of alphas in TFTR.[24–26] The dynamics of this effect is complicated,[27] but a simple model has been incorporated into TRANSP.[3] The effect of sawtooth crashes on the fast alpha density computed by TRANSP is shown in Fig. 17. The recovery of the alpha fusion

TABLE IV. Beam-driven and bootstrap currents with 50 MW D-NBI.

Current (MA)	Flat n_e (01001A03)	Peaked n_e (01002A07)
I_{beam}	0.7	0.6
I_{boot}	3.1	5.6
I_{OH}	17.2	14.8
I_{total}	21.0	21.0

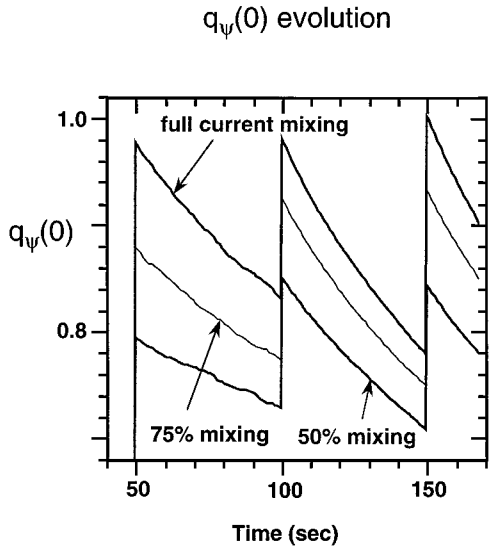

FIG. 15. Evolution of $q_\psi(0)$ with alternative assumptions about the fraction of current mixing during sawteeth crashes.

power and alpha heating profiles will depend on details of how the temperatures and the D, T, impurities, and alpha densities are redistributed, and how the transport evolves since these determine the subsequent reheating.

VI. RIPPLE EFFECTS

The fast-ion ripple losses are estimated in TRANSP by assuming the ions are lost if their turning points are in regions with ripple exceeding an empirical factor times the Goldston–White–Boozer (GWB)[28] threshold. The simple GWB estimate has recently been improved[29] but the improvement has not yet been installed into TRANSP. The threshold has been renormalized[8] by comparing losses obtained[7] with TRANSP and with the Hamiltonian guiding-center code ORBIT.[10] The thresholds that give agreement for

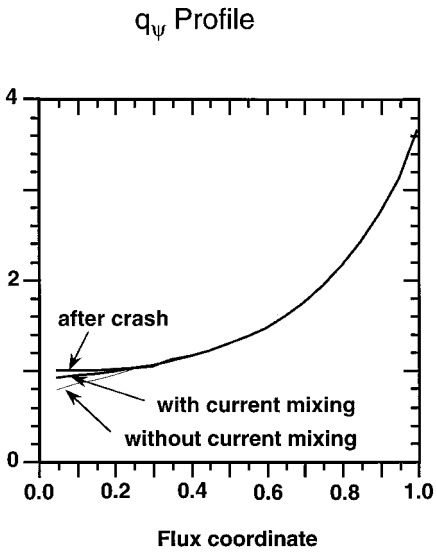

FIG. 16. Computed q_ψ profiles with alternative assumptions about the fraction of current mixing during sawteeth crashes.

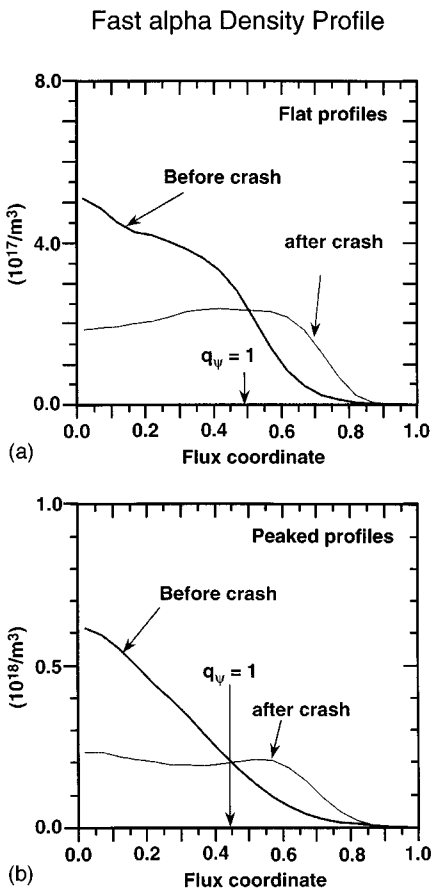

FIG. 17. Computed change in the fast alpha density during sawteeth crashes for (a) the flat density profile case, and (b) the peaked density profile case.

TFTR supershots are 1/2*GWB for the fast alpha particles and 4*GWB for the beam ions. The actual threshold renormalization is strongly collisionally dependent on the artificial pitch angle acceleration level used in TRANSP.[8] Similar renormalization for ITER discharges with appropriately higher statistics indicates that the threshold for alpha particles is near 1/2*GWB (as in TFTR), not 1*GWB.[29] In the case of ITER, this reduction is due to the asymmetry of the equilibrium and the geometry.

The prediction for the steady state phases of the peaked-profile ITER discharge is that 3% of the alpha energy and 4% of the fast alpha particles are ripple lost. A comparable fraction of the beam ion energy is expected to be ripple lost. If the fast alphas are redistributed by sawtooth crashes, the ripple loss is expected to increase. With the flat redistribution shown in Fig. 17(b), the ripple loss is predicted to increase by a factor of 3.[29] The duration of this increased loss depends on the dynamics of recovery of the alpha profile to the pre-crash state. This depends on unknown details of the plasma recovery. Ripple losses from the flat profile discharge are expected to be slightly larger since the alpha particle density is broader (Fig. 8).

VII. ALPHA ASH

The transport coefficients of the thermal ash were varied to determine values that generate equilibrium ash profiles consistent with 1.5 GW of fusion power. The diffusivity and radial pinch velocity profiles for the ash density are defined from their density and net flux profiles

$$\gamma_{\mathrm{He}} = -D_{\mathrm{He}}\ \mathrm{grad}(n_{\mathrm{He}}) + V_{\mathrm{He}} n_{\mathrm{He}}. \tag{1}$$

In steady state, the volume integral to the separatrix of the thermal He ion density is given by

$$\frac{dN_{\mathrm{He}}}{dt} = S_{\mathrm{th}} + \Gamma_{\mathrm{in}} - \Gamma_{\mathrm{out}} = S_{\mathrm{th}} - \Gamma_{\mathrm{pump}} = 0 \tag{2a}$$

with Γ_{out} the He flux out through the separatrix surface, Γ_{in} the (neutral) He flux returning back from the scrape off or divertor regions to the core through the separatrix surface, and S_{th} is the volume integral of the alpha thermalization rate. The fluxes are related by

$$\Gamma_{\mathrm{in}} = R_{\mathrm{rec}} \Gamma_{\mathrm{out}}, \tag{2b}$$

$$\Gamma_{\mathrm{pump}} = (1 - R_{\mathrm{rec}}) \Gamma_{\mathrm{out}}, \tag{2c}$$

with R_{rec} the average recycling coefficient *at the separatrix surface,* and Γ_{pump} the rate with which He must be removed from the region within the separatrix. TRANSP calculates the alpha thermalization rate profiles to be close to the DT fusion rate, as shown in Fig. 8.

The global He confinement times at the separatrix are defined as:

$$\tau_{\mathrm{He}} = N_{\mathrm{He}} / \Gamma_{\mathrm{out}}, \tag{3a}$$

$$\tau^*_{\mathrm{He}} = N_{\mathrm{He}} / \Gamma_{\mathrm{pump}} = \tau_{\mathrm{He}} / (1 - R_{\mathrm{rec}}). \tag{3b}$$

Some of the He ''ash'' parameters have been measured in present day tokamas. For instance, results from experiments with TFTR supershots indicate that n_{He} is relatively flat compared with n_e.[31] The transport coefficients consistent with these measurements have $D_{\mathrm{He}}(x) \approx D_e(x) \approx \chi_{\mathrm{eff}}(x)$ (the effective energy transport coefficient). The radial pinch $V_{\mathrm{He}}(x)$ has relatively small values for $x < 0.5$, and anomalously large negative values for $x > 0.6$. The recycling coefficient consistent with these measurements is $R_{\mathrm{rec}} \cong 0.85$, and the ratio $\tau^*_{\mathrm{He}} / \tau_E \cong 6$.

It is not clear how the existing tokamak results scale to ITER discharges. For instance, the intense central fueling from NBI in present experiments can cause more peaking of n_e than expected in ITER. Also, $D_e \ll \chi_{\mathrm{eff}}$ might be expected in ITER [see Fig. 13(b)], but $D_{\mathrm{He}} \ll \chi_{\mathrm{eff}}$ would imply large accumulations of He ash. Because of these uncertainties, a range of He transport coefficients is studied here. It is inefficient to use TRANSP to scan in the ratio $D_{\mathrm{He}}/\chi_{\mathrm{eff}}$ since χ_{eff} changes as the n_{He}/n_e ratio and the alpha heating change. A simpler assumption is used here: scans with constant D_{He} and V_{He} are studied. For most of the runs the pinch is assumed to be negligible.

Another uncertainty for ITER is the value of R_{rec}. Apparently the average He recycling coefficient near the pumps will be very close to 1.0. The interim design for ITER specifies an effective pumping speed of 100–300 m^3/s.[1] This speed times the neutral density or pressure at the pump ducts gives the total pumping rate. A high neutral pressure is desired to increase the pumping rate. This pressure must be supported by the scrape off flow to the divertor and flux

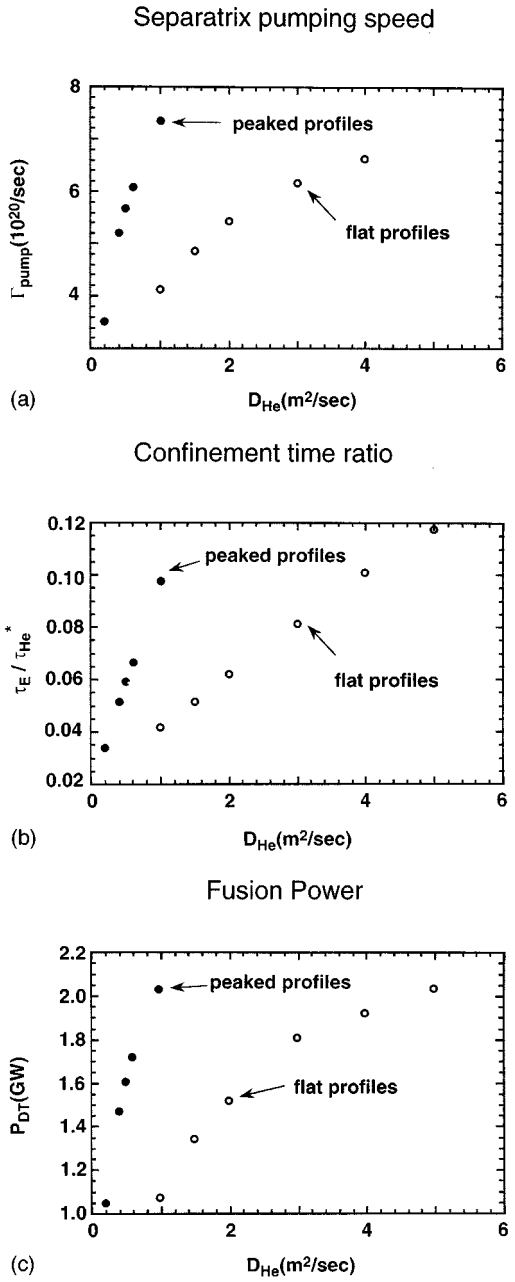

FIG. 18. Dependencies of (a) He pumping, (b) the ratio τ_{He}/τ_E, and (c) the ratio τ_E/τ_{He}^*, if $R_{rec}=0.5$ and $V_{He}=0$.

amplification (reionization increasing the ion flux) near the divertor region. High flux amplification near the divertor keeps the density of He in the separatrix low and R_{rec} low. At fixed He transport coefficients, this lowers the He density in the plasma, increasing the fusion power at fixed electron density and temperatures. High values for R_{rec} lead to pessimistic requirements for the He transport coefficients to achieve 1.5 GW fusion power. We first discuss results derived using an intermediate value ($R_{rec}=0.5$), and then indicate how the requirements change as R_{rec} varies.

Each TRANSP run used a fixed D_{He} and V_{He} and initial conditions chosen to speed the convergence to steady state n_{He} profiles. One measure of equilibrium is $S_{th}/\Gamma_{pump}=1$ [see Eq. 2(a)]. The runs reported here converged sufficiently so

TABLE V. Thermal He parameters for $P_{DT}=1.5$ GW if $R_{rec}=0.5$ and $V_{He}=0$.

Parameter	Flat n_e (01001A03)	Peaked n_e (01002A07)
D_{He} (m^2/s)	2	0.4
V_{He} (m/s)	0	0
$n_{He}(0)/n_e(0)$	0.14	0.15
$n_{He}(1)/n_e(1)$	0.16	0.32
N_{He} (10^{22})	3.65	4.18
Γ_{pump} (10^{20}/s)	5.4	5.2
τ_{He} (s)	33.5	40.1
τ_{He}^* (s)	67	80

that $S_{th}/\Gamma_{pump}=1$ to within 8%. As D_{He} increases, N_{He}, τ_{He}, and τ_{He}^* decrease, whereas Γ_{pump} and P_{DT} increase. These dependencies are shown in Fig. 18. For the flat profile case shown in Fig. 13(a), D_{He} needs to be at least 2 m^2/s to achieve 1.5 GW in steady state, which is comparable to χ_{eff} near $x=0.5$. For the peaked case in Fig. 13(b), D_{He} needs to be at least 0.4 m^2/s, which is considerable lower than χ_{eff} with NBI.

Ash parameters are summarized in Table V. As D_{He} increases, τ_E/τ_{He}^* increases. The corresponding increase in P_{DT} is shown in Fig. 19. This ratio needs to be smaller than about 15 to achieve $P_{DT}=1.5$ GW with the plasma and recycling we assume.

For the runs discussed above, D_{He} is varied with R_{rec} fixed at 0.5 and V_{He} fixed at zero. If instead, P_{DT} is held fixed, and R_{rec} is varied, the value of Γ_{pump} in Eq. (2c) remains fixed, so Γ_{out} varies as $1/(1-R_{rec})$. For instance, if R_{rec} increases from 0.5 to 0.95, the value of D_{He} needed to achieve 1.5 GW increases by a factor of 10. The required upper bound on τ_E/τ_*^{He} remains around 15. Thus if the pinch is negligible, the required D_{He} increases from 2 to 20 m^2/s for the flat profile case and from 0.4 to 4 m^2/s for the peaked profile case. These required values are much higher than those measured in present tokamaks. Clearly low values for R_{rec} are desired.

As $-V_{He}$ increases, larger values of D_{He} are needed to keep n_{He} low enough to achieve 1.5 GW. Profiles of n_{He} generated by several combinations of D_{He} and V_{He} that are

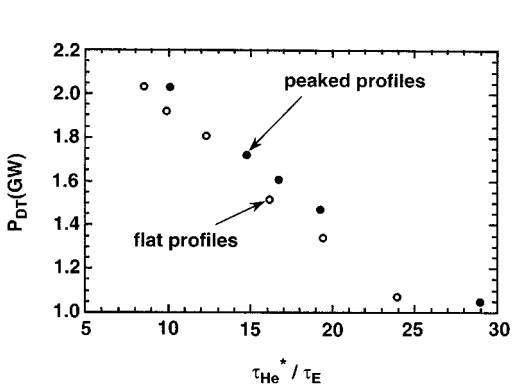

FIG. 19. Dependence of the fusion power on the ratios of (a) τ_E/τ_{He}^*, and (b) τ_{He}^*/τ_E if $R_{rec}=0.5$ and $V_{He}=0$.

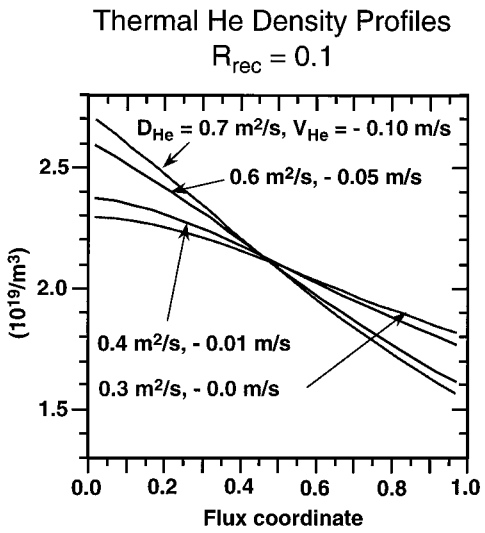

FIG. 20. Examples of D_{He} and V_{He} that produce steady state n_{He} profiles for the peaked n_e case with $P_{\mathrm{DT}}=1.5$ GW and $R_{\mathrm{rec}}=0.10$. When $-V_{\mathrm{He}}$ is large, both the D_{He} and V_{He} terms in Eq. (1) are large with opposite signs.

consistent with $R_{\mathrm{rec}}=0.10$ and 1.5 GW are shown in Fig. 20. The V_{He} profiles are assumed to have constant values for $x<0.9$ and to increase linearly to 0.0 at the boundary ($x=1$). The corresponding values of D_{He} are low compared with the values required if $R_{\mathrm{rec}}=0.5$.

VIII. SUMMARY

The TRANSP plasma analysis code is used to model the steady state phases (including periodic sawteeth) of two discharges from the ITER database. TRANSP provides comprehensive, self-consistent models for the particle, energy, and momentum balance, and computes thermal transport coefficients and alpha parameters. Several models for the transport of thermal ion species are available. The model for the relative mixing of D and T that is consistent with TFTR measurements gives pessimistic results for ITER with D-NBI. Results assuming equal D and T transport are assumed here. Effects of 50 MW of D-NBI at 1 MeV are studied. The heating occurs over most of the plasma, and the average energy of the beam ions is approximately one-half the injection energy. The beam-driven currents are $\sim$0.6 MA for this voltage. The beam ions contribute significantly to the ion and electron heating in the region around $x=0.8$.

The $q_\psi=1$ radius is calculated to occur near the $x=0.25$–0.5 flux surface. The amount of current mixing and the sawtooth period significantly effect the $q_\psi(0)$ value. Sawteeth crashes are modeled to significantly redistribute the fast ion density profiles.

Steady state toroidal field ripple is estimated to cause losses of $\sim$3% of the alpha energy and $\sim$4% of the fast alpha particles from the peaked profile discharge. If the fast alphas are redistributed by sawtooth crashes, the ripple losses are predicted to increase by about a factor of three transiently.

The alpha ash is modeled assuming constant transport coefficients with a range of values. The ratio of the confinement times, $\tau^*_{\mathrm{He}}/\tau_E$ needed to achieve steady state fusion powers of 1.5 GW with the assumed electron density and ion temperature profiles is $\leqslant$15. The required ash diffusivity D_{He} depends strongly on the pinch and the average recycling coefficient at the separatrix surface, R_{rec}. If the pinch is negligible and if $R_{\mathrm{rec}}\leqslant 0.5$, then values of D_{He} comparable to those measured in present tokamak experiments is sufficient. If R_{rec} is much larger, then higher values are needed. Accurate edge and scrape-off modeling is needed for more accurate estimates of R_{rec}.

ACKNOWLEDGMENTS

We wish to thank D. Boucher, S. Kaye, M. Rosenbluth, R. White, and S. Zweben for discussions and encouragement.

This work is supported by the U. S. Department of Energy under Contract No. DE-AC02-76CH0-3073.

[1] *Technical Basis for the ITER Interim Design Report, Cost Review and Safety Analysis* (International Atomic Energy Agency, Vienna, 1996).
[2] P. H. Rebut, V. Chuyanov, M. Huguet, R. R. Parker, Y. Shimomura, and the ITER Joint Central Team and Home Teams, in *Fifteenth International Conference on Plasma Physics and Controlled Nuclear Fusion Research*, Seville, Spain, 1994 (International Atomic Energy Agency, Vienna, 1995).
[3] Available on Internet at http://picard.iterus.org.
[4] R. V. Budny, M. G. Bell, R. E. Bell, J. L. Jassby, L. C. Johnson, D. K. Mansfield, D. C. McCune, M. H. Redi, J. F. Schivell, G. Taylor, T. B. Terpstra, M. C. Zarnstorff, and S. J. Zweben, Nucl. Fusion **35**, 1497 (1995).
[5] R. V. Budny, G.-Y. Fu, N. N. Gorelenkov, J. Manickam, M. P. Petrov, M. H. Redi, S. Sabbagh, R. B. White, L. Zakharov, Y. Zhao, and S. J. Zweben, ''Occurrence of sawteeth in ITER and their effects on alpha particles and stability,'' in *23rd European Physical Society Conference on Controlled Fusion and Plasma Physics*, Kiev (European Physical Society, Petit-Lancy, 1996), Vol. 1, pp. 55–58.
[6] D. C. McCune, R. J. Goldston, R. T. McCann, R. M. Wieland, T. B. Terpstra, B. Balet, and P. Stubberfield, Bull. Am. Phys. Soc. **39**, 1680 (1994).
[7] M. H. Redi, M. C. Zarnstorff, R. B. White, R. V. Budny, A. C. Janos, D. K. Owens, J. F. Shivell, S. D. Scott, and S. J. Zweben, Nucl. Fusion **35**, 1191 (1995).
[8] M. H. Redi, R. V. Budny, D. S. Darrow, H. H. Duong, R. K. Fisher, A. C. Janos, J. M. McChesney, D. C. McCune, S. S. Medley, M. P. Petrov, J. F. Schivell, S. D. Scott, R. B. White, M. C. Zarnstorff, and S. J. Zweben, Nucl. Fusion **35**, 1509 (1995).
[9] M. H. Redi, R. V. Budny, D. S. Darrow, A. C. Janos, D. C. McCune, S. S. Medley, J. Shivell, S. D. Scott, R. B. White, M. C. Zarnstorff, S. J. Zweben, and the TFTR group, in *22nd European Physical Society Conference on Controlled Fusion and Plasma Physics*, Bournemouth (European Physical Society, Petit-Lancy 1995), Vol. II, p. 105.
[10] R. B. White and M. Chance, Phys. Fluids **27**, 2455 (1984); R. B. White, Phys. Fluids B **2**, 845 (1990).
[11] R. C. Grimm, R. W. Dewer, and J. Manickam, J. Comput. Phys. **49**, 94 (1983).
[12] C. Z. Cheng, G. Y. Fu, H. E. Mynick, R. V. Budny, R. B. White, S. J. Zweben, C. T. Hsu, D. J. Sigmar, D. A. Spong, B. A. Carreas, and C. L. Hendrick, *Fourteenth International Conference on Plasma Physics and Controlled Nuclear Fusion Research*, Würzburg, 1992 (International Atomic Energy Agency, Vienna, 1993).
[13] R. V. Budny, M. G. Bell, H. Biglari, M. Bitter, C. E. Bush, C. Z. Cheng, E. D. Fredrickson, B. Grek, K. W. Hill, A. C. Janos, D. L. Jassby, D. W. Johnson, B. LeBlanc, D. C. McCune, D. R. Mikkelsen, H. K. Park, A. T. Ramsey, S. A. Sabbagh, S. D. Scott, J. F. Schivell, J. D. Strachan, B. C. Stratton, E. J. Synakowski, G. Taylor, M. C. Zarnstorff, and S. J. Zweben, Nucl. Fusion **32**, 429 (1992).
[14] B. Balet, P. M. Stubberfield, D. Borba, J. G. Cordey, N. Deliyanakjis, C. M. Greenfield, T. T. C. Jones, R. Konig, F. B. Marcus, M. F. F. Nave, D. P. O'Brien, F. Porcelli, G. J. Sadler, K. Thomsen, and M. Von Hellermann, Nucl. Fusion **33**, 1345 (1993).
[15] B. LeBlanc, S. M. Kaye, N. Asakura, R. E. Bell, P.-A. Duperrex, G. M. Gammel, H. Fishman, R. E. Hatcher, A. Holland, P. Kaita, C. E. Kessel, H. W. Kugel, F. M. Levinton, M. Okabayashi, S. F. Paul, N. R. Sauthoff,

S. Sesnic, and H. Takahashi, Nucl. Fusion **33**, 1645 (1993).
[16]J. Ongena, H. Conrads, M. Gaigneaux, A. M. Messiaen, R. R. Weynants, E. Barbian, G. Bertschinger, P. Borgermans, R. V. Budny, T. Delvigne, P. Dumortier, F. Durodie, H. G. Esser, H. Euringer, G. Fuchs, B. Giesen, E. Graffmann, D. L. Hillis, F. Hoenen, P. Huttemann, M. Jadoul, H. Kever, R. Koch, W. Kohlhaas, L. Konen, M. Korten, H. R. Koslowski, A. Kramer-Flecken, M. Lochter, G. Mank, A. Plspieszczyk, U. Samm, B. Schweer, H. Soltwisch, G. Telesca, R. Uhlemann, P. E. Vandenplas, R. Van Nieuwenhove, G. Van Oost, M. Vervier, G. Van Wassenhove, G. Waidmann, J. Winter, and G. H. Wolf, Nucl. Fusion **33**, 283 (1993).
[17]G. T. Hoang, C. Gil, E. Joffrin, D. Moreau, A. becoulet, P. Bibet, J. P. Bizarro, R. V. Budny, J. Carrasco, J. P. Coulon, C. De Michelis, T. Dudok de Wit, P. Monier-Garbet, M. Goniche, R. Guirlet, T. Hutter, S. M. Kaye, J. LaSalle, L. Laurent, P. Lecoustey, X. Litaudon, M. Mattioli, Y. Peysson, A.-L. Pecquet, G. Rey, S. S. Sabbagh, B. Saoutic, G. Tonon, and J. C. Vallet, Nucl. Fusion **34**, 75 (1994).
[18]M. Greenwald, R. L. Boivin, P. Bonoli, C. Christensen, C. Fiore, D. Garnier, J. Goetz, S. Golovato, M. Graf, R. Granetz, S. Horne, T. Hsu, A. Hubbard, I. Hutchinson, J. Irby, C. Kurz, B. LaBombard, B. Lipschultz, T. Luce, E. Marmar, G. McCracken, A. Niemczewski, P. O'Shea, M. Poeklab, J. Rice, J. Reardon, J. Scharchter, J. Snipes, P. Stek, Y. Takase, J. Terry, M. Umansky, R. Watterson, and S. Wolfe, Phys. Plasmas **2**, 2308 (1995).
[19]R. V. Budny, L. Grisham, D. L. Jassby, J. Manickam, D. McCune, K. M. McGuire, S. A. Sabbagh, S. D. Scott, D. Stotler, R. Wieland, M. C. Zarnstorff, and S. J. Zweben, *Proceedings of the 19th European Conferencee on Plasma Physics and Controlled Fusion*, Innsbruck, European Conference on Plasma Physics and Controlled Fusion 1992 (European Physical Society, Petit-Lancy, 1993), Vol. I, p. 43.
[20]R. V. Budny, Nucl. Fusion **34**, 1247 (1994).
[21]R. V. Budny, M. Bitter, H. H. Duong, Q. Gao, G. T. Hoang, D. Jassby, L. C. Johnson, B. LeBlanc, S. von Goeler, A. T. Ramsey, C. H. Skinner, and D. P. Stotler, ''Tritium influx and transport in Tokamak Fusion Test Reactor plasmas with deuterium neutral beam injection,'' submitted to Phys. Plasmas.
[22]F. Porcelli, D. Boucher, and M. N. Rosenbluth, in *22nd European Physical Society Conference on Controlled Fusion and Plasma Physics*, Bournemouth (European Physical Society, Petit-Lancy 1995), Vol. III, p. 169.
[23]M. Yamada, F. M. Levinton, N. Pomphrey, R. Budny, J. Manickam, and Y. Nagayama, Phys. Plasmas **1**, 3269 (1994).
[24]R. Fisher, J. M. McChesney, P. B. Parks, H. H. Duong, S. S. Medley, A. L. Roquemore, D. K. Mansfield, R. V. Budny, M. P. Petrov, and R. E. Olson, Phys. Rev. Lett. **75**, 846 (1995).
[25]M. Petrov, R. V. Budny, H. H. Duong, R. K. Fisher, N. N. Gorelenkov, J. M. McHesney, D. K. Mansfield, S. S. Medley, P. B. Parks, M. H. Redi, and A. L. Roquemore, Nucl. Fusion **35**, 1437 (1995).
[26]M. P. Petrov, N. N. Gorelenkov, R. V. Budny, Z. Chang, D. S. Darrow, H. H. Duong, R. K. Fisher, R. J. Fonck, H. W. Herrmann, G. R. McKee, S. S. Medley, A. Odblom, A. L. Roquemore, B. C. Stratton, F. Wising, R. B. White, Y. Zhao, and S. J. Zweben, ''Sawtooth mixing of alpha particles in TFTR D-T plasmas,'' to appear in *Proceedings of the 1996 IAEA Conference*, Montreal (International Atomic Energy Agency, Vienna, in press).
[27]Y. Zhao and R. White ''Simulation of alpha particle redistribution due to sawteeth in TFTR,'' submitted to Phys. Plasmas.
[28]R. J. Goldston, R. B. White, and A. H. Boozer, Phys. Rev. Lett. **47**, 647 (1981).
[29]R. White, R. J. Goldston, M. H. Redi, and R. V. Budny, Phys. Plasmas **3**, 3043 (1996).
[30]M. H. Redi, R. J. Golsston, R. B. White, R. V. Budny, D. McCune, and C. O. Miller, ''TF ripple loss of alpha particles from the ITER Interim Design: Simulation and theory,'' in *23nd European Physical Society Conference on Controlled Fusion and Plasma Physics*, Kiev, 1996 (European Physical Society, Petit-Lancy, in press).
[31]E. J. Synakowski, R. E. Bell, R. V. Budny, C. E. Bush, P. C. Efthimion, B. Grek, D. W. Johnson, L. C. Johnson, B. LeBlanc, A. T. Ramsey, and G. Taylor, Phys. Rev. Lett. **75**, 3689 (1995).